



Title	Long-Range Order Parameter of Oriented L1 ₀ -FePt Nanoparticles Determined by Electron Diffraction
Author(s)	Sato, Kazuhisa; Hirotsu, Yoshihiko
Citation	Materials Transactions. 2003, 44(8), p. 1518-1522
Version Type	VoR
URL	https://hdl.handle.net/11094/89446
rights	
Note	

The University of Osaka Institutional Knowledge Archive : OUKA

<https://ir.library.osaka-u.ac.jp/>

The University of Osaka

Long-Range Order Parameter of Oriented L1₀-FePt Nanoparticles Determined by Electron Diffraction

Kazuhisa Sato and Yoshihiko Hirotsu

The Institute of Scientific and Industrial Research (ISIR-SANKEN), Osaka University, Ibaraki 567-0047, Japan

Two-dimensionally dispersed L1₀-FePt nanoparticles as small as 12 nm with orientation was fabricated by electron-beam evaporation and post-annealing at 873 K. After a prolonged annealing at 873 K for 86.4 ks, the increase of coercivity was almost saturated and coercivity reached 434 kAm⁻¹ at 300 K, which is very small compared to recent reports on FePt nanoparticles with sizes larger than 20 nm. Long-range order parameter of the fabricated nanoparticles was determined by electron diffraction at 200 kV taking the multiple scattering into consideration. Obtained order parameter remained 0.55 ± 0.02 for the nanoparticles with an axial ratio c/a of 0.961 ± 0.003 . The low degree of order is thought to be responsible for the small coercivity. Effect of Debye-Waller factor on the order parameter was discussed.

(Received April 14, 2003; Accepted May 16, 2003)

Keywords: FePt, nanoparticle, electron diffraction, $hh0$ systematic reflection, dynamical scattering, order parameter, multi-slice simulation

1. Introduction

Magnetic properties of nanoparticles have been studied because of their scientific and industrial interests.¹⁾ In these years, nanoparticles of L1₀-type FePt ordered alloy are now attracting much interests for their potential applications to future high-density magnetic storage media, since the FePt alloy has a high thermal stability of magnetization due to a large magnetocrystalline anisotropy²⁾ as well as a large saturation magnetization compared to CoPtCr-based alloys.³⁾ The large magnetocrystalline anisotropy constant (K_u) of L1₀-FePt alloy is originated from its tetragonal ordered structure. In this sense, there are several reports on the relation between K_u and long-range order parameter (S),⁴⁻⁷⁾ and a gradual decrease of K_u with S has been reported for FePt thin films.⁵⁻⁷⁾ These S values have been determined by X-ray diffraction using integrated intensities of fundamental and superlattice reflections based on the kinematical scattering theory.⁸⁾ According to recent reports on FePt granular films,⁹⁻¹¹⁾ their particle sizes reached a few ten nanometer or less in diameter. Recently, the authors have reported a formation of L1₀ ordered phase even in 2-nm-sized FePt nanoparticles,¹²⁾ which was characterized by high-resolution transmission electron microscopy (HREM) and electron diffraction. We also measured magnetic hysteresis of L1₀-FePt nanoparticles with mean size of 5 nm, and obtained a coercivity of 32 kAm⁻¹ at 10 K.¹²⁾ Thermal fluctuation of magnetization is thought to be less significant at 10 K, so the magnetoanisotropy for the smaller nanoparticles must be decreased due to lower degree of order. Coercivity measured at 300 K increased with particle size and exceeded 80 kAm⁻¹ when particle size became larger than about 9 nm.¹³⁾ For 12-nm-sized FePt particles, increase of coercivity saturated after annealing at 873 K for 86.4 ks. However, coercivity still remained 434 kAm⁻¹ at 300 K,¹⁴⁾ which is very small compared to the recent reports on 50-nm-sized FePt nanoparticles¹⁵⁾ with coercivities of about 3.2 MA m⁻¹ at 300 K. Investigation of the relation between the particle size and the order parameter is necessary for explaining the small coercivity of very small FePt nanoparticles, however, a reduction of particle size (ie: reduction of particle volume)

causes a broadening of diffracted intensity, which leads to a difficulty in evaluating the accurate integrated intensity from conventional X-ray diffraction profiles.

In the case of transmission electron diffraction by using fast electrons, the scattering power of atoms for electrons is about 10⁴ times larger than that for X-rays.¹⁶⁾ So electron diffraction has a great advantage in obtaining superstructure reflections from L1₀-FePt nanoparticles,^{12,17)} especially for an assembly of oriented nanoparticles with two-dimensional dispersion. However, the dynamical scattering effect makes analysis of electron diffraction intensity significantly difficult. The multi-slice approach is known as a useful method for calculating the intensity of electrons propagating through crystals.¹⁸⁻²⁰⁾ Transmitted and diffracted beam intensities after the multiple scattering (dynamical scattering) can be evaluated precisely by multi-slice simulation when such experimental parameters as specimen thickness, incident beam direction, specimen composition, lattice parameter and temperature factor (Debye-Waller factor: B) are known in addition to the crystal structure.

The authors have been fabricating oriented FePt nanoparticles with two-dimensional dispersion on substrate surface.²¹⁾ Such nanoparticle specimens are thought to be suitable for the determination of S by electron diffraction compared to FePt granular films with a three-dimensional particle dispersion and a random orientation. For a precise determination of the order parameter, a consideration of several experimental and numerical parameters is necessary. In this study, epitaxially grown hard magnetic isolated L1₀-FePt nanoparticles as small as 12 nm were prepared. The long-range order parameter of the particles has been determined precisely by electron diffraction taking account of the multiple scattering effect.

2. Experimental

2.1 Specimen fabrication and characterization

FePt nanoparticles were fabricated by successive deposition of Pt and Fe onto both cleaved NaCl and MgO(001) substrates kept at 673 K. We took advantage of the overgrowth of Fe nanoparticles onto Pt "seed" nanoparticles,²¹⁾

which were epitaxially grown on the substrate surface. Post-deposition annealing at 873 K for 86.4 ks was performed in order to promote the alloying and the atomic ordering reaction of Fe and Pt. The deposited average thickness was set to be about 1 nm both for Fe and Pt, which resulted in a formation of isolated FePt nanoparticles with a mean particle size of 12 nm in diameter. The orientation relationships observed by electron diffraction are as follows: $\langle 100 \rangle_{\text{Fe}} \parallel \langle 100 \rangle_{\text{Pt}}$, $\{011\}_{\text{Fe}} \parallel \{010\}_{\text{Pt}}$. After the deposition of Fe, we further deposited amorphous Al₂O₃ film in order to protect the particles from oxidation and also to avoid the particles coalescence on annealing. Details of fabrication procedure are shown in our previous article.²¹⁾ Structure and morphology of FePt nanoparticles were characterized by transmission electron microscopy (TEM) and selected area electron diffraction (SAED) operated at 200 kV (JEOL, JEM-2010). Magnetic properties were measured by a SQUID magnetometer (Quantum Design, MPMS-5S). Compositional analysis was performed by energy dispersive X-ray spectroscopy (EDS) in TEM (JEOL, JEM-3000F). The present Fe–Pt specimens have an average composition of 56 at%Pt.

2.2 Evaluation of long-range order parameter by electron diffraction intensity analysis

The definition of the order parameter is as follows:⁸⁾

$$S = \frac{r_\alpha - x_A}{y_\beta} = \frac{r_\beta - x_B}{y_\alpha}, \quad (1)$$

where r_α (r_β), x_A (x_B), and y_α (y_β) denote the fraction of α -sites (β -sites) occupied by the right atom, the atom fractions represent alloy composition, and the fractions of α -sites (β -sites), respectively. In evaluating the S value in X-ray diffraction, the integrated intensity ratio of the fundamental and the superlattice reflections is measured. In the present electron diffraction, the ratio of the 110 superlattice and 220 fundamental reflections has been also used to evaluate the S value of the L1₀-FePt nanoparticles. Because of the nanoparticles with fixed orientations, the intensity ratio I_{110}/I_{220} strongly depends on the film orientation in SAED. For convenience, we confined the beam incidence parallel to the optical axis (namely, all the diffracted intensities for hkl reflections almost appear as $I_{hkl} = I_{\bar{h}\bar{k}\bar{l}}$ in the present structure). In the evaluation of the S value, $hh0$ systematic reflections were excited in the electron diffraction experiment. In the electron diffraction experiments, SAED patterns with both of the [001] and $[\bar{1}16]$ beam incidences were recorded using Imaging Plates (IP, Fuji Film, FDL-UR-V) for later quantitative analysis of diffracted beam intensities under different exposure times ranging from 4 to 64 sec. In the reading process of IP after the recording of SAED patterns, we considered the fading effect of IP.²²⁾ Because of the strong electron scattering in the L1₀-FePt lattice, multiple scattering (dynamical scattering) is inevitable even in the case of small sized FePt nanoparticles. In order to evaluate the I_{hh0} diffraction intensities correctly, I_{hh0} intensity calculations have been performed using the multi-slice method. Transmitted and diffracted beam intensities were calculated based on the multi-slice simulation using a computer software, “Mac Tempas” ppc. The space group of L1₀ structure is P4/

Table 1 Numerical parameters used for multi-slice calculations.

Alloy	Fe–Pt
Composition	56 at%Pt
Space group	P4/mmm
Lattice constant	$a = 0.386$, $c = 0.371$ nm
Temperature factor (B)	0.003, 0.01 nm ²
Accelerating Voltage	200 kV
Spherical aberration	0.5 mm
Absorption (Imaginary Potential)	10% of Real Potential
Aperture (G_{max})	30 nm ^{−1}
Slice thickness	0.1 nm
Zone axis	$[\bar{1}16]$, [001]

mmm, which gives the following structure factors of reflection, $F_{hkl} = 2(f_{\text{Fe}} + f_{\text{Pt}})$ for hkl unmixed and $F_{hkl} = 2|f_{\text{Fe}} - f_{\text{Pt}}|$ for hkl mixed. Numerical parameters used in this calculation are listed in Table 1. In the calculation, we limited reflections up to a spatial frequency of 30 nm^{−1}, ($= 1/d_{hkl}$: d_{hkl} is the interplane spacing for (hkl) plane). Lattice parameters used here were determined from the SAED patterns using a Pt thin film mounted on a Cu grid as “standard” for the camera-length correction. The measured lattice parameters were $a = 0.386 \pm 0.001$ and $c = 0.371 \pm 0.001$ nm with axial ratio c/a of 0.961 ± 0.003 . The average thickness of FePt particles was set to be 7 nm, which was estimated by a cross-sectional TEM observation. The accurate value of B for 12-nm-sized FePt nanoparticles is not known, so we took $B = 0.003$ nm² after the values for bulk metals.^{23,24)}

3. Results

3.1 Structure and morphology of the oriented L1₀-FePt nanoparticles

As-deposited specimens were composed of nano-complex particles of bcc-Fe and Pt. Annealing of these specimens at the temperatures above 773 K lead to a formation of ordered FePt nanoparticles with the L1₀-type structure. In our previous study, the oriented L1₀-FePt nanoparticles formed by annealing at 873 K with annealing time up to 21.6 ks were composed of three-variant structural domains with respect to the tetragonal symmetry of the L1₀-structure.²¹⁾ On further prolonged annealing at 873 K, the three-variant structural domains decomposed into single variant nanoparticles with their three possible directions of c -axes normal or parallel to the film plane.¹⁴⁾ Figures 1(a) and (b) show the HREM images and the corresponding SAED pattern for Fe–56 at%Pt nanoparticles after annealing at 873 K for 86.4 ks. Single domain nanocrystal (single domain) particles are seen with their c -axes oriented both normal and parallel to the film plane, which results in an appearance of both 001 and 110 superlattice reflections in the SAED pattern with the $\langle 100 \rangle$ incidence.

3.2 Evaluation of the order parameter

We determined the order parameter using the intensities of 110 and 220 reflections. In the following, determination of S

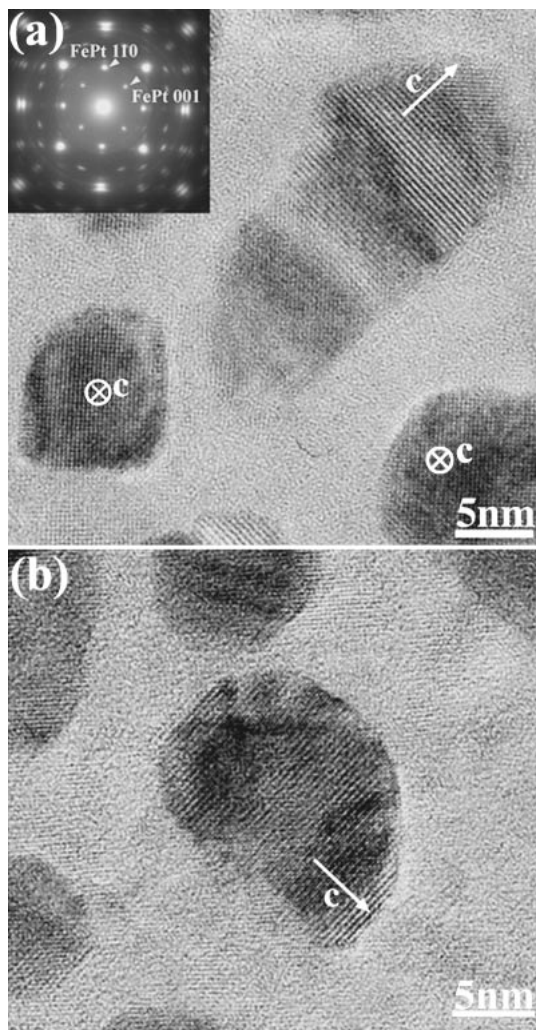


Fig. 1 HREM images and the corresponding SAED pattern for Fe₄₄Pt₅₆ nanoparticles after annealing at 873 K for 86.4 ks. Nanoparticles with *c*-axis oriented normal and parallel to the film plane are seen in (a) and (b), respectively.

for this specimen is presented. A slight beam tilting from [001] incidence, for example, $[\bar{1}14]$ or $[\bar{1}16]$ incidence, results in an excitation of $hh0$ systematic reflections, which reduces diffracted beams and can largely decrease and simplify the multiple scattering events among the transmitted and the diffracted waves. For [001] incidence, the intensity ratio I_{110}/I_{220} shows complicated dependence of specimen thickness even below 10 nm thick, while in the case of $[\bar{1}16]$ incidence, the intensity ratio increases monotonically. By tilting the specimen about 0.23 rad from the [001] incidence towards the $[\bar{1}10]$ direction, we can excite the $hh0$ systematic reflections in the SAED pattern with beam incidence of $[\bar{1}16]$ as shown in Fig. 2. In the figure, the 110 and 220 reflection spots are indicated by the single arrow heads. The double arrow head indicates the 022 (and/or 202) reflection spot due to the existence of three kinds of *c*-axis orientation of the nanoparticles in the specimen. Since these reflections come from different particles with different *c*-axis orientations and also these particles are two dimensionally distributed on the α -Al₂O₃ film, no phase relation exists, nor any double diffraction occurs between these reflections. In Fig. 2, 220 reflections show slight arc along the circumference direction,

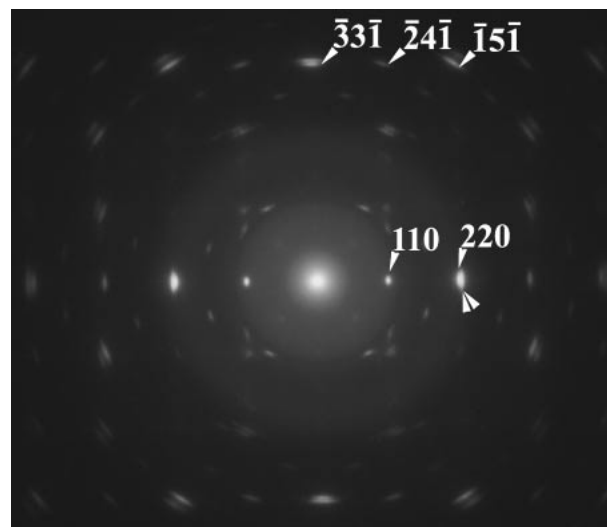


Fig. 2 A SAED pattern with beam incidence of $[\bar{1}16]$. Excitation of the $hh0$ systematic reflections is seen. Besides the 110 and 220 reflection spots, 022 (and/or 202) reflection spot is also seen (indicated by double arrow head).

indicating a slight rotation of FePt nanoparticles on the substrate crystals. However, such a slight rotation on the substrate surface does not affect the I_{110}/I_{220} intensity ratio in the case of $[\bar{1}16]$ incidence. The 110 and 220 intensities shown in Fig. 2 were measured as digital intensity data recorded in IP. The 220 and 202 (and/or 022) reflection profiles were separated by means of Lorentzian fitting. Here, a full width of half maximum (FWHM) of the 110 superlattice reflection, 0.14 nm^{-1} , was used. The obtained intensity ratio, I_{110}/I_{220} , was 0.54 ± 0.03 .

In order to evaluate the order parameter for the present specimen, we need a relation between the calculated I_{110}/I_{220} ratio and the order parameter value. The relation on the basis of the multi-slice simulation is shown in Fig. 3 under the average particle thickness of 7 nm. Dotted line shows experimentally obtained I_{110}/I_{220} value. Using the relation

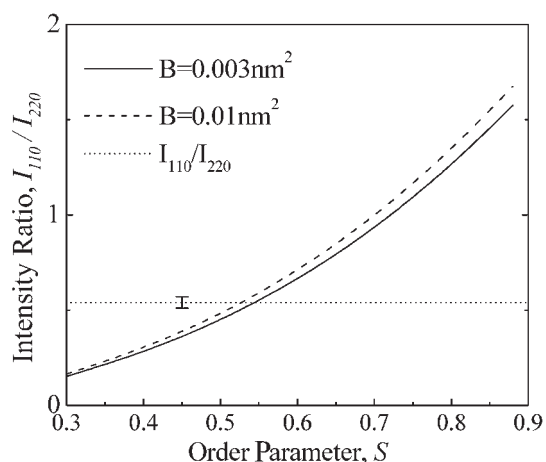


Fig. 3 Order parameter dependence of intensity ratio I_{110}/I_{220} obtained by the multi-slice simulations. Solid and broken lines are the results obtained under the B values of 0.003 and 0.01 nm^2 , respectively. Dotted line indicates the experimentally obtained intensity ratio I_{110}/I_{220} of 0.54 ± 0.03 .

in Fig. 3, the order parameter is determined as 0.55 ± 0.02 . Then we examined the effect of thickness dependence on the order parameter. Particle thickness distribution was estimated to have a log-normal type distribution function with $\ln \sigma = 0.39$, which was assumed from the particle size distribution. Considering the above particle thickness distribution, the average order parameter is expressed as follows:

$$\bar{S} = \sum_i S(t_i) \cdot n(t_i), \quad (2)$$

where $S(t_i)$ denotes the order parameter of the i -th particle with the thickness t_i and $n(t_i)$ the fraction of the thickness. The summation was performed in the range of 7 ± 1.5 nm based on the deviation of $\ln \sigma = 0.39$. Obtained average order parameter was 0.56, which is almost the same value as that of evaluated using an average thickness of 7 nm.

4. Discussion

The temperature factor used in this article was 0.003 nm^2 both for Fe and Pt in the present multi-slice calculations. According to the International Tables for X-ray Crystallography,²³⁾ the B values for bulk metals are tabulated, where $B = 0.0035$ or 0.0018 nm^2 for Fe and $B = 0.0028$ or 0.0022 nm^2 for Pt at 293 K. Butt and Bashir²⁴⁾ presented a compilation of recommended B values at 293 K. In their list, $B = 0.0035$ and 0.0032 nm^2 are presented for bulk Fe and Pt, respectively. These are the bases for using the B of 0.003 nm^2 in this study. In the assembly of FePt nanoparticles, the temperature factor may be different from that of the bulk FePt alloy due to the thermal vibration. There are several reports showing the increase of B with decreasing the particle size.^{25–31)} Harada and Ohshima²⁵⁾ reported the temperature factor for Au particles, where the B value is about 0.01 nm^2 at 300 K for 15 nm-sized Au particles ($B = 0.0062$ or 0.0040 nm^2 ,²³⁾ or 0.0057 nm^2 ²⁴⁾ at 293 K for bulk Au). They also showed that their obtained B for Au particles with sizes 6 to 23 nm included scarcely the static components. Ohshima *et al.*²⁶⁾ reported the B of 0.0118 nm^2 for 2-nm-sized Pd particles ($B = 0.0032$ or 0.0036 nm^2 ,²³⁾ or 0.0045 nm^2 ²⁴⁾ for bulk Pd). Kashiwase *et al.*²⁷⁾ reported the B of 0.018 nm^2 for 3-nm-sized Cr particles ($B = 0.0028$ ²³⁾ or 0.0026 nm^2 ²⁴⁾ for bulk Cr). Crescenzi *et al.*,²⁸⁾ and Telgheder and Urban²⁹⁾ reported the size dependence of B for Cu clusters at 300 K, where obtained maximum value of B was about 0.01 nm^2 for 2-nm-sized clusters. In the present study, the mean particle size is 12 nm in diameter, so it is considered that the used B value of 0.003 nm^2 is thought to be valid considering the above results. We also calculated the intensity ratio under the large B value of 0.01 nm^2 , and obtained the S of 0.53 ± 0.02 under the average particle thickness of 7 nm, which is 3.6% smaller than that of obtained by the calculation performed under the B of 0.003 nm^2 .

Present specimen of FePt nanoparticles showed a coercivity of 434 kAm^{-1} at 300 K¹⁴⁾ after a sufficient annealing. Estimated saturation magnetization (I_s) was 1.35 T using the averaged thickness of Fe and Pt which was monitored by quartz oscillator during the deposition. Here, we estimated the magnetoanisotropy constant at 300 K for the present FePt

nanoparticles as $1.2\text{--}1.4 \times 10^6 \text{ Jm}^{-3}$ based on the Pfeiffer's equation³²⁾ assuming the random orientation of particles. The estimated magnetoanisotropy constant coincides in order with the values of FePt thin films^{6,7)} with the order parameter of about 0.5. However, the estimated magnetoanisotropy constant includes not only magnetocrystalline anisotropy but also surface and/or shape contributions. Shima *et al.*¹⁵⁾ reported the decrease of anisotropy constant with decreasing the average FePt nanoparticle size. So it is concluded that the smaller nanoparticle sizes cause lower degree of order and reduce the magnetoanisotropy constant of the present FePt nanoparticles to give a smaller coercivity. Concerning the atomic ordering of FePt granular films, Takahashi *et al.* have recently discussed the decrease of the order-disorder transformation temperature with particle size.³³⁾

5. Conclusion

Long-range order parameter of two-dimensionally distributed Fe₄₄Pt₅₆ nanoparticles as small as 12 nm with orientation was determined as 0.55 ± 0.02 by measuring electron diffraction 110 and 220 intensities from $hh0$ systematic reflections with the help of multi-slice intensity calculation under the B value of 0.003 nm^2 . Even by using the B value of 0.01 nm^2 , which is larger than that for bulk materials, the order parameter decreased only 3.6%. From the coercivity and the saturation magnetization, we estimated the magnetoanisotropy constant to be $1.2\text{--}1.4 \times 10^6 \text{ Jm}^{-3}$. The lower degree of order and isolated small nanoparticles morphology are responsible for the relatively smaller K_u value of the present FePt nanoparticles compared with that of the bulk L1₀-FePt alloy. Determination of S by electron diffraction has a great advantage for nanometer-sized materials, where conventional X-ray diffraction is thought to be difficult.

Acknowledgements

This study was supported by the Center of Excellence (COE) Program at ISIR-SANKEN, Osaka University, Grant-in-Aid for Scientific Research (Nos. 14205094, 13555189 and 13750612) and Special Coordination Funds for Promoting Science and Technology on "Nanohetero metallic materials" from the Japanese Ministry of Education, Culture, Sports, Science and Technology. This study was partly supported by Research Foundation For Materials Science.

REFERENCES

- 1) J. L. Dormann and D. Fiorani (ed.): *Magnetic Properties of Fine Particles*, (Elsevier, Amsterdam, 1992) pp. 93–177.
- 2) O. A. Ivanov, L. V. Solina, V. A. Demshila and L. M. Magat: *Phys. Met. Metallogr.* **35** (1973) 81–85.
- 3) D. Weller and M. F. Doerner: *Annu. Rev. Mater. Sci.* **30** (2000) 611–644.
- 4) V. V. Maykov, A. Ye. Yermakov, G. V. Ivanov, V. I. Khrabrov and L. M. Magat: *Phys. Met. Metallogr.* **67** (1989) 76–82.
- 5) S. Mitani, K. Takanashi, M. Sano, H. Fujimori, A. Osawa and H. Nakajima: *J. Magn. Magn. Mater.* **148** (1995) 163–164.
- 6) H. Kanazawa, G. Lauhoff and T. Suzuki: *J. Appl. Phys.* **87** (2000) 6143–6145.
- 7) S. Okamoto, N. Kikuchi, O. Kitakami, T. Miyazaki, Y. Shimada and K. Fukamichi: *Phys. Rev. B* **66** (2002), 024413.1–024413.9.

- 8) B. E. Warren: *X-ray Diffraction*, (Dover, New York, 1990) pp. 208–210.
- 9) C. P. Luo and D. J. Sellmyer: *Appl. Phys. Lett.* **75** (1999) 3162–3164.
- 10) S. Sun, C. B. Murray, D. Weller, L. Folks and A. Moser: *Science* **287** (2000) 1989–1992.
- 11) Z. R. Dai, S. Sun and Z. L. Wang: *Surf. Sci.* **505** (2002) 325–335.
- 12) K. Sato, M. Fujiyoshi, M. Ishimaru and Y. Hirotsu: *Scr. Mater.* **48** (2003) 921–927.
- 13) K. Sato, T. Kajiwaru, M. Fujiyoshi, M. Ishimaru, Y. Hirotsu and T. Shinohara: *J. Appl. Phys.* **93** (2003) 7414–7416.
- 14) K. Sato, B. Bian, T. Hanada and Y. Hirotsu: *Scr. Mater.* **44** (2001) 1389–1393.
- 15) T. Shima, K. Takanashi, Y. K. Takahashi and K. Hono: *Appl. Phys. Lett.* **81** (2002) 1050–1052.
- 16) P. Hirsch, A. Howie, R. Nicholson, D. W. Pashley and M. J. Whelan: *Electron Microscopy of Thin Crystals*, (Krieger, Florida, 1977) pp. 90–91.
- 17) K. Kaneko, S. Matsumura, K. Ikematsu, Y. Kato, Y. Tomokiyo, M. Watanabe and T. Masumoto: *Scr. Mater.* **48** (2003) 915–920.
- 18) P. M. J. Fisher: *Jpn. J. Appl. Phys.* **7** (1968) 191–199.
- 19) J. M. Cowley: *Diffraction Physics*, 3rd revised ed., (Elsevier, Amsterdam, 1995) pp. 189–253.
- 20) P. Buseck, J. M. Cowley and L. Eyring (ed.): *High-Resolution Transmission Electron Microscopy and Associated Techniques*, (Oxford, New York, 1992) pp. 245–259.
- 21) B. Bian, K. Sato, Y. Hirotsu and A. Makino: *Appl. Phys. Lett.* **75** (1999) 3686–3688.
- 22) T. Oikawa, D. Shindo and K. Hiraga: *J. Electron Microsc.* **43** (1994) 402–405.
- 23) K. Lonsdale (ed.): *International Tables for X-ray Crystallography*, Vol. III (The Kynoch Press, Birmingham, 1962), pp. 232–244.
- 24) N. M. Butt and J. Bashir: *Acta Cryst. A* **44** (1988) 396–398.
- 25) J. Harada and K. Ohshima: *Surf. Sci.* **106** (1981) 51–57.
- 26) K. Ohshima, S. Yatsuya and J. Harada: *J. Phys. Soc. Jpn.* **50** (1981) 3071–3074.
- 27) Y. Kashiwase, I. Nishida, Y. Kainuma and K. Kimoto: *J. Phys. Soc. Jpn.* **38** (1975) 899.
- 28) M. De Crescenzi, M. Diociaiuti, L. Lozzi, P. Picozzi and S. Santucci: *Phys. Rev. B* **35** (1987) 5997–6003.
- 29) F.-W. Telgheder and J. Urban: *J. Electron Spectroscopy and Related Phenomena* **95** (1998) 267–279.
- 30) A. V. Chadwick, N. V. Russell, A. R. Whitham and A. Wilson: *Sensors and Actuators B* **18–19** (1994) 99–102.
- 31) J.-F. Lee, M.-T. Tang, W. C. Shih and R. S. Liu: *Mater. Res. Bull.* **37** (2002) 555–562.
- 32) H. Pfeiffer: *Phys. Status Solidi (a)* **118** (1990) 295–306.
- 33) Y. K. Takahashi, T. Ohkubo, M. Ohnuma and K. Hono: *J. Appl. Phys.* **93** (2003) 7166–7168.